Discovery of a pre-cataclysmic binary with unusual chromaticity of the eclipsed white dwarf by the GPX survey

Krushinsky, V., Benni, P., Burdanov, A., Antokhin, I., Antokhina, E., Jehin, E., Barkaoui, K., Fitzsimmons, A., Gibson, C., Gillon, M., Popov, A., Baştürk, Ö., Benkhaldoun, Z., Marchini, A., Papini, R., Salvaggio, F., & Brazhko, V. (2020). Discovery of a pre-cataclysmic binary with unusual chromaticity of the eclipsed white dwarf by the GPX survey. *Monthly Notices of the Royal Astronomical Society*, *493*(4), 5208-5217. https://doi.org/10.1093/mnras/staa547

Document Version:
Peer reviewed version

Queen's University Belfast - Research Portal:
Link to publication record in Queen's University Belfast Research Portal

Discovery of a pre-cataclysmic binary with unusual chromaticity of the eclipsed white dwarf by the GPX survey

Krushinsky, V., Benni, P., Burdanov, A., Antokhin, I., Antokhina, E., Jehin, E., Barkaoui, K., Fitzsimmons, A., Gibson, C., Gillon, M., Popov, A., Baştürk, Ö., Benkhaldoun, Z., Marchini, A., Papini, R., Salvaggio, F., & Brazhko, V. (2020). Discovery of a pre-cataclysmic binary with unusual chromaticity of the eclipsed white dwarf by the GPX survey. *Monthly Notices of the Royal Astronomical Society*, *493*(4), 5208-5217. https://doi.org/10.1093/mnras/staa547

Discovery of a pre-cataclysmic binary with unusual chromaticity of the eclipsed white dwarf by the GPX Survey

Vadim Krushinsky[1]⋆, Paul Benni[2], Artem Burdanov[3,4], Igor Antokhin[5], Eleonora Antokhina[5], Emmanuël Jehin[6], Khalid Barkaoui[7,8], Alan Fitzsimmons[9], Christopher Gibson[9], Michaël Gillon[7], Alexander Popov[1], Özgür Baştürk[10], Zouhair Benkhaldoun[8], Alessandro Marchini[11], Riccardo Papini[12], Fabio Salvaggio[12], Varvara Brazhko[1]

[1] *Ural Federal University, 620002, Mira Street, 19, Yekaterinburg, Russian Federation*
[2] *Acton Sky Portal (Private Observatory), Acton, MA, USA*
[3] *Department of Earth, Atmospheric and Planetary Sciences, Massachusetts Institute of Technology, 77 Massachusetts Avenue, Cambridge, MA 021*
[4] *Instituto de Astrofísica de Canarias, Vía Láctea s/n, 38205 La Laguna, Tenerife, Spain*
[5] *Moscow Lomonosov State University, Sternberg State Astronomical Institute, 119992 Universitetsky prospect, 13, Moscow, Russian Federation*
[6] *Space Sciences, Technologies and Astrophysics Research (STAR) Institute, Université de Liège, Allée du 6 Août 19C, 4000 Liège, Belgium*
[7] *Astrobiology Research Unit, Université de Liège, Allée du 6 Août 19C, 4000 Liège, Belgium*
[8] *Oukaimeden Observatory, High Energy Physics and Astrophysics Laboratory, Cadi Ayyad University, Marrakech, Morocco*
[9] *Astrophysics Research Centre, Queen's University Belfast, Belfast BT7 1NN, Northern Ireland*
[10] *Ankara University, Faculty of Science, Department of Astronomy and Space Science, TR-06100 Tandogan, Ankara, Turkey*
[11] *Astronomical Observatory - DSFTA, University of Siena, Via Roma 56, 53100 Siena, Italy*
[12] *Wild Boar Remote Observatory, San Casciano in Val di Pesa (FI), Italy*

ABSTRACT

We report the discovery of a relatively bright eclipsing binary system, which consists of a white dwarf and a main sequence K7 star with clear signs of chromospheric and spot activity. The light curve of this system shows ∼ 0.2 mag ellipsoidal variability with a period of 0.297549 d and a short total eclipse of the white dwarf. Based on our analysis of the spectral and photometric data, we estimated the parameters of the system. The K7V star is tidally deformed but does not fill its Roche lobe (the filling factor is about 0.86). The orbital inclination is $i = 73°.1 \pm 0°.2$, the mass ratio is $q = M_2/M_1 \approx 0.88$. The parameters of the K7V star are $M_2 \approx 0.64\,M_\odot$, $R_2 = 0.645 \pm 0.012\,R_\odot$, $T_2 \approx 4070$ K. The parameters of the white dwarf are $M_1 \approx 0.72\,M_\odot$, $R_1 = 0.013 \pm 0.003\,R_\odot$, $T_1 = 8700 \pm 1100$ K. Photometric observations in different bands revealed that the maximum depth of the eclipse is in the *SDSS r* filter, which is unusual for a system of a white dwarf and a late main sequence star. We suspect that this system is a product of the evolution of a common envelope binary star, and that the white dwarf accretes the stellar wind from the secondary star (the so-called low-accretion rate polar, LARP).

Key words: binaries: close – binaries: eclipsing – stars: white dwarfs – stars: low mass

1 INTRODUCTION

A stellar binary, which consists of a white dwarf (WD) primary and a main sequence (MS) secondary star is referred

---

⋆ E-mail: krussh@gmail.com

to as WDMS and it is a result of the evolution of the system of two MS stars, where one of the companions turns into the WD. A WDMS system evolves from an initially wider binary system, where the primary companion evolves into a red giant forming a common envelope containing the less massive and, therefore, less evolved secondary companion (Willems & Kolb 2004). During the common envelope phase, stars transfer orbital angular momentum to the surrounding matter, what causes decrease of the orbital separation between them. Later, the common envelope is ejected from the system and a WDMS system is formed (Paczynski 1976). Such systems are denoted as post common envelope binaries (PCEB). If components of the WDMS have small orbital separation, gravity of the WD distorts the secondary companion. As a result, one can observe an ellipsoidal modulation of the light curve due to the change of the observed area of the secondary. Other periodical modulations occur because of the temperature gradient of the secondary due to gravitational darkening, absorption and reflection of radiation emitted by the WD. Further angular momentum loss occurs due to various mechanisms (magnetic braking, gravitational wave radiation, etc.), and separation decreases until the secondary overflows Roche lobe and the WDMS turns into a cataclysmic variable (e.g., Knigge et al. 2011). When the projected distance between the centres of the companions (impact parameter) is favourable, then eclipses might be observed. In this case, a depth of the eclipse depends on a size of the WD and its temperature relative to the secondary companion. In a simple black-body model, if the WD is hotter than the MS, the eclipse depth monotonically increases from IR to UV (e.g., see SDSS J030308.35+005444.1 light curve from Parsons et al. 2013b).

WDMS systems are favourable objects for observations and studies, as possible progenitors of cataclysmic variables and as benchmarks for testing stellar evolutionary models. Eclipsing WDMS systems make it possible to infer the absolute sizes and masses of companions and also make it possible to test the WD mass-radius relationship (Parsons et al. 2017). Thanks to the extensive modern surveys like SDSS (York et al. 2000) and CRTS (Drake et al. 2009), numerous eclipsing WDMS systems have been discovered (e.g., Parsons et al. 2013a, 2015), but eclipsing systems still represent a minor part of the known population of WDMS systems (Ren et al. 2018). Exoplanet transit surveys, in turn, also expand the current population of eclipsing WDMSs. For example, Maxted et al. (2014) reports on the discovery of 17 new eclipsing WDMS systems from the ground-based WASP survey (Pollacco et al. 2006) and Faigler et al. (2015) describes discoveries of new short-period eclipsing systems with low-mass WDs from *Kepler* light curves (Borucki et al. 2010).

Based on the prototype KPS survey (Burdanov et al. 2016), the Galactic Plane eXoplanet survey (GPX, Benni 2017; Burdanov et al. 2018) performs photometric observations of the Galactic plane to search for new transiting exoplanets. However, all the stars are routinely scanned for any signs of variability. In this paper, we present the discovery of GPX-TF16E-48 variability in the GPX wide-field data and attempt to explain the peculiar photometric behaviour of this eclipsing WDMS system using additional photometric and spectroscopic observations.

The rest of the paper is structured as follows: Section 2

describes GPX discovery wide-field photometry, subsequent follow-up observations with different instruments and data reduction. Section 3 is devoted to the light curve and spectral analysis. In Section 4 we discuss the results obtained and make assumptions about the nature of this eclipsing binary. In the Section 5 we outline our findings.

2   DISCOVERY AND FOLLOW-UP OBSERVATIONS

2.1   GPX detection photometry and open source data

The TF16E field of the GPX survey was observed with the RASA telescope from 2018 August 5 to 2018 October 22 for 27 nights in the R_c filter. The RASA telescope is a Rowe-Ackermann Schmidt Astrograph (0.28-m, f/2.2) wide-field telescope and it is the main instrument of the GPX wide-field exoplanet search. It is based at the Acton Sky Portal private observatory in Acton (MA, USA) and it was built from readily available off-the-shelf equipment. GPX-TF16E-48's photometric light curve was automatically selected as a possible variable star using our automatic reduction pipeline. The pipeline includes standard photometric and astrometric (Lang et al. 2010) reductions, flux extraction using IRAF (Tody 1993), differential photometry using close ensemble of comparison stars and search for objects with significant variability. Identification of variable stars is based on the RoMS (Robust Median Statistics) criterion, described in Rose & Hintz (2007). A detailed description of the pipeline is provided in Burdanov et al. 2014, 2016. Indeed, the target's light curve shows variability, typical to W Ursae Majoris-type eclipsing variables (EW) with an amplitude of 0.175 mag and a period of 7.14 h ($\sim$ 0.3 d). However, the light curve had a few surprises: a box-shaped eclipse with an amplitude of 0.06 mag is seen and the positions of the maxima of the main 0.175 mag variability are slightly shifted from -0.25 and $+0.25$ phases. The discovery light curve folded with the 7.14 h period is shown in Fig. 1, where the occurring box-shaped eclipse has 0.00 phase.

The Gaia DR2 parallax of the object is 5.137 ± 0.0194 mas, which corresponds to a distance of 194.7 ± 0.7 pc (Gaia Collaboration et al. 2018). The colour indices and apparent magnitudes from different catalogues match with a K7-M1 dwarf located at 100-200 pc. There are several magnitude measurements from Pan-STARRS PS2 (Chambers et al. 2016), which are in agreement with the observed variability from the GPX survey. GPX-TF16E-48 is a faint UV source in the NASA/IPAC Extragalactic Database (NED), and it is not presented in any X-ray database. The main variability of the object was independently detected by Vitali Nevski using ASAS-SN database and added to the VSX database on 2018 December 14 as an EW variable star[1].

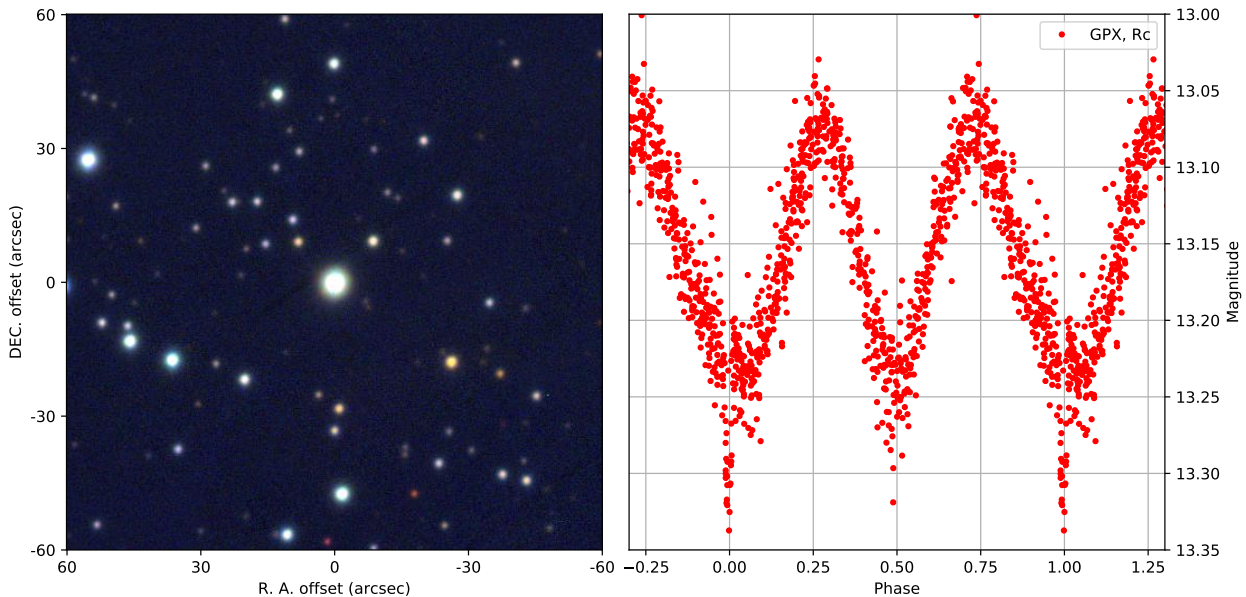We summarize all the information about GPX-TF16E-48 in Table 1 and provide a finding chart in Fig.1

---

[1] https://www.aavso.org/vsx/index.php?view=detail.top&oid=629066

Figure 1. Left: PanStarrs-1 colour (i/r/g) image of the 2′x2′ area around GPX-TF16E-48. Right: GPX discovery light curve folded with the 7.14 h period.

Table 1. General information about GPX-TF16E-48. B and V magnitudes are from the APASS catalog (Henden et al. 2015), J magnitude – from the 2MASS catalog (Skrutskie et al. 2006).

Identifiers	GPX-TF16E-48
	Gaia DR2 531486745299867904
	2MASS 01294349+6715300
	VSX NEV239
RA (J2000)	01h 29m 43.488s
DEC (J2000)	+67° 15′ 30.02″
Gaia parallax	5.137±0.0194 mas
Bmag	15.936
Vmag	14.713
Jmag	11.953
Period	0.297549 ± 0.000001 d
Epoch(HJD)	2458762.2285 ± 0.0005

2.2 Follow-up observations

Photometric follow-up observations of GPX-TF16E-48 were carried out with seven telescopes at five observatories (see Table 2 for a summary). Short time-series before, during and after the eclipse, and during the opposite phase were obtained with the TRAPPIST-North telescope (Barkaoui et al. 2017; Jehin et al. 2011; Gillon et al. 2011) in November and December 2018 in the B, V, R_C, narrow-band Hα and I+z bands. High precision observations of the eclipse in the B filter were obtained on 2018 November 30 with the SAI MSU 2.5-m telescope (Potanin et al. 2017). Simultaneous observations covering the full period were obtained using the Kourovka 1.2-m telescope in the V band on 2019 April 4 and in the *SDSS g, r* and *i* bands on 2019 April 9-10 (Fig. 2) and October 7 using a three-channel CCD photometer.

The TÜBİTAK National Observatory T100 telescope,

MASTER-Ural (Lipunov et al. 2010) and Acton Sky Portal 14″SCT telescopes observed GPX-TF16E-48 for several nights in 2018 and 2019 in different filters (see Table 2).

Photometric reductions were performed in a standard way using dark frames and twilight sky flat-field images. Fluxes were extracted with the aperture photometry technique using fixed aperture radius ∼1.5 FWHM, where FWHM is the mean full width at half maximum of the stellar point spread function (PSF) during the observing run. We used an ensemble of nearby non-variable stars with similar to the GPX-TF16E-48 colour indices to derive the target's differential light curve and we checked all reference stars light curves for possible correlations with airmass, pixel position, FWHM and sky background.

Four spectra of the GPX-TF16E-48 star were obtained with the Isaac Newton Telescope/Intermediate Dispersion Spectrograph (INT/IDS) on 2018 December 14 and 17. These observations correspond to phases −0.196, −0.156, −0.074 and 0.339 (Fig. 3). All exposures were 900 seconds long and a slit width of 1.0″ was used. The seeing varied for different exposures and on 2018 December 17 there was a considerable amount of dust in the atmosphere. The spectra were reduced using the standard INT/IDS pipeline. The wavelength calibration is accurate to 0.1Å (rms) or better for all spectra. The pixel scale in the data is ∼1.5Å per pixel, so wavelength calibration is better than 0.1 pixel. Radial velocities measurements are provided in Table 3.

Photometric and spectroscopic data are available for download from the Kourovka Observatory file sharing server.[2]

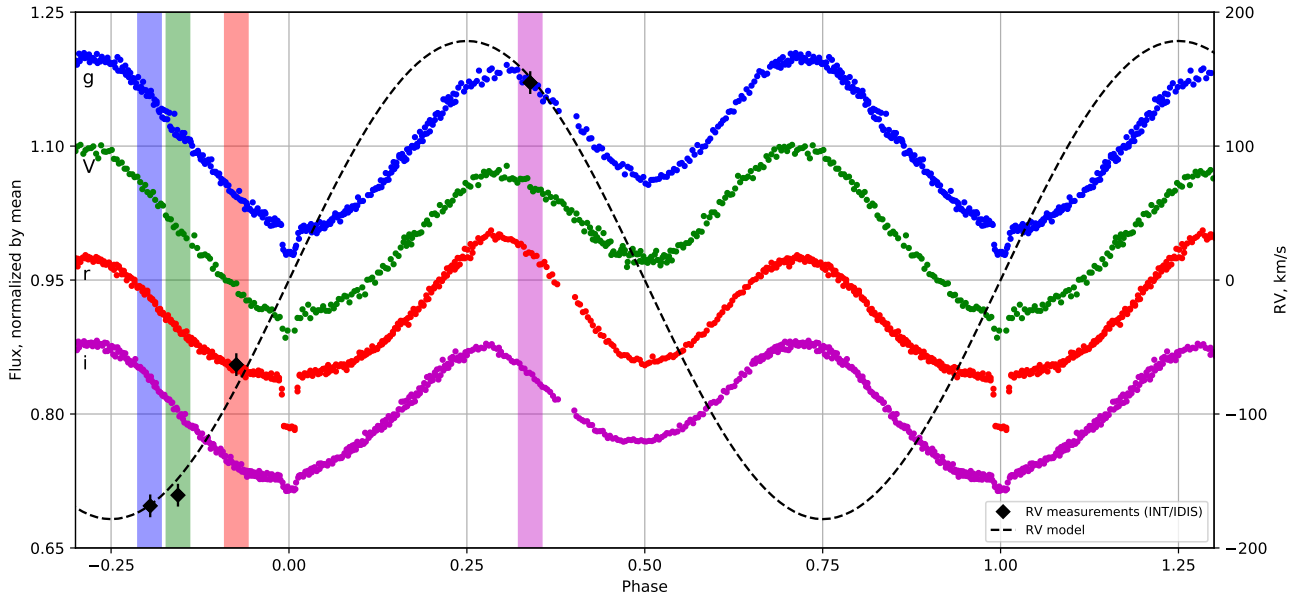[2] https://optlab.kourovka.ru/GPX_TF16_48/

Figure 2. Period-folded light curves of GPX-TF16E-48 (left axis) and radial velocity measurements (right axis). Photometric data obtained on 2019 April with the Kourovka 1.2-m telescope (see Subsection 2.2 for details). All light curves were normalised and shifted vertically by 0.1 for visual clarity. Colours of vertical stripes corresponded to colours of spectra on Fig. 3, and their widths are equal to exposure time.
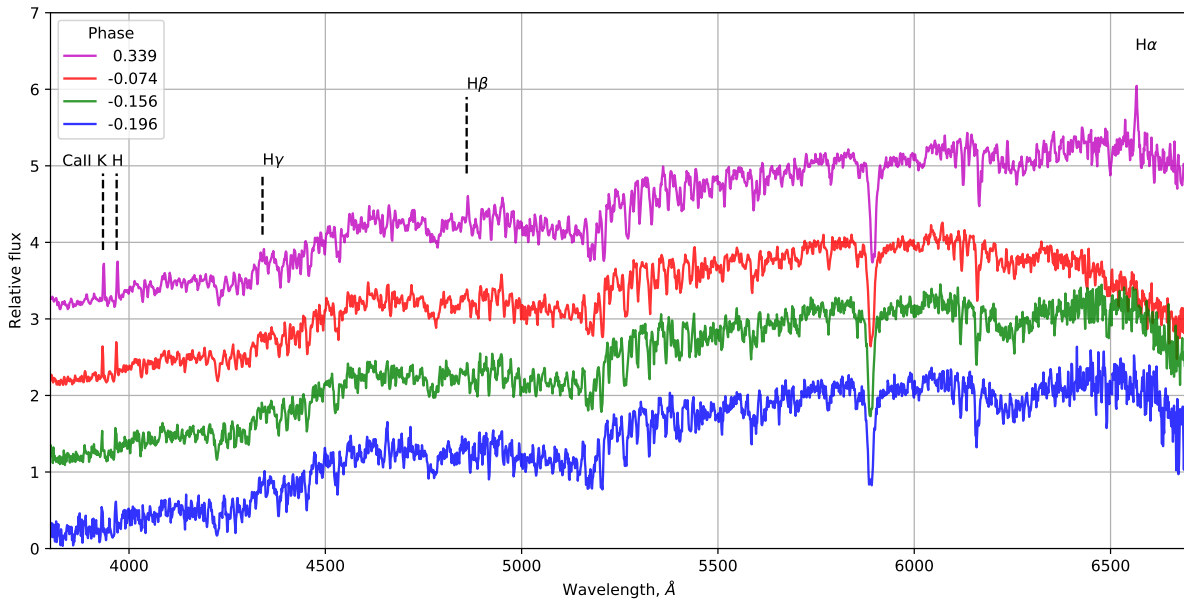
Figure 3. Four spectra were obtained with the Isaac Newton Telescope/Intermediate Dispersion Spectrograph on 2018 December 14 and 17. Strong Ca II H-K emissions are present in all spectra. The Balmer lines are clearly visible on phase 0.339. All spectra were obtained at same zenith distance (43–41°) but in different weather and seeing condition (see Subsection 2.2 for details). Spectra were normalized to the mean flux in 4000–5000 Å region and shifted vertically for visual clarity. The bend of continuum near 6500 Å on phase −0.074 is due to data reduction issues.

Table 2. Follow-up observations log

Observatory	Telescope	Date	Filters/Dispersion	Comments
Acton Sky Portal	RASA, 0.28-m, f/2.2	Aug.-Oct. 2018	R_c	22 nights, discovery light curve
Acton Sky Portal	Celestron, 0.35-m, f/11	Nov.-Dec. 2018	g, r, i	6 nights, follow-up observations
Oukaïmeden	TRAPPIST-North, 0.6-m, f/8	Nov.-Dec. 2018	B, V, R_c, I+z, Hα	5 observations of the eclipse in different bands
Kourovka	1.2-m, f/10	Apr., Oct. 2019	V, g, r, i	3+1 nights of high S/N observations simultaneous observations in g, r an
Kourovka	MASTER, 0.4-m, f/2.5	Jan.-Apr. 2019	V, R	18 nights; simultaneous observations in V and R
TÜBİTAK	T100, 1.0-m, f/10	18 Feb. 2019	I	Observations of one period
CMO SAI MSU	2.5-m, f/10	30 Nov. 2018	B	High S/N observation of the eclipse
Roque de los Muchachos	INT/IDS, 2.5-m	14 and 17 Dec. 2018	3800–6700 Å, 1.5 Å/pix.	4 low resolution spectra

Table 3. Measured radial velocities of K7V companion

Obs. midpoint (BJD)	Phase	Barycentric RV ($km\,s^{-1}$)
2458467.29929651	-0.196	-205 ± 9
2458467.31110172	-0.156	-197 ± 9
2458470.31100902	-0.074	-99 ± 9
2458470.43392171	0.339	111 ± 9

3 DATA ANALYSIS

Ephemeris of GPX-TF16E-48 were determined using a period search service WEBEFK[3] based on the Lafler-Kinman method (Lafler & Kinman 1965) and are given in Table 1.

Spectral classification of the red dwarf component of GPX-TF16E-48 was done by comparing the spectra with the spectral library (Valdes et al. 2004). We determined the spectral class as K7V, which is in agreement with the Gaia parallax. Strong Ca II H-K emissions are present in all spectra, indicating significant chromospheric activity of the MS companion (Wilson 1968). Balmer emission lines are clearly visible on the phase 0.339. Velocities of the emission lines correspond to the red dwarf companion. We did not detect any obvious spectral signs of the WD in the spectra. A library spectrum of HD237903 was used as a template for cross-correlation measurements of the radial velocities. The semi-amplitude of radial velocity is $K_2 = 178 \pm 10\,km\,s^{-1}$ and it was obtained under the assumption of a circular orbit.

The ingress and egress of the total eclipse are $\sim 100\,s$ long and the full duration of the eclipse is only $600\,s$ (Fig. 4). Based on the shape of the light curve and total eclipse, we assumed that the system consists of a MS star with a large Roche lobe filling factor and a WD. The maximum temperature of the WD should not exceed $10\,000\,K$ from the low flux in the *GALEX* FUV and NUV and the depths of the eclipse in different bands (Fig. 4, right panel).

3.1 Light curves modelling

The light curves of GPX-TF-16E-48 clearly show significant ellipsoidal variability and a short total eclipse of the compact object with rather small amplitude. Similar light curves have been observed in RR Caeli (Bruch & Diaz 1998) and

[3] http://vast.sai.msu.ru/lk/

SDSS 0303+0054 (Pyrzas et al. 2009), which were classified as post-common envelope binaries consisting of a WD and a MS star. The ellipsoidal variability of RR Caeli and SDSS 0303+0054 is notably smaller than that of GPX-TF-16E-48 ($\sim 0.2\,mag$), which clearly indicates that in the latter case, the MS star is strongly deformed and (nearly) fills its critical Roche lobe. To estimate the stellar and orbital parameters of the system, we performed an analysis of four light curves, fully covering the orbital period, and observed with the 1.2-m Kourovka telescope: V band (2019 April 4) and *SDSS g*, *r*, and *i* bands (2019 April 9). The amplitudes of the total eclipse of the WD are equal to $\sim 0.04\,(g)$, $\sim 0.03\,(V)$, $\sim 0.07\,(r)$, $\sim 0.03\,mag\,(i)$ (see Fig. 5, right panels). The light curves are notably asymmetric, the fluxes of the two maxima are different, the ingress and egress parts of the primary ellipsoidal minimum are also asymmetric. Also, if only ellipsoidal variability was present, its depth around the orbital phase 0.0 would be smaller than that at the phase 0.5. These features indicate the presence of spot(s) on the surface of the MS star (Tappert et al. 2007; Parsons et al. 2016; Latković et al. 2019).

The analysis was performed with our own code for synthesis of light and radial velocity curves of close binary systems (CBSs) in the Roche model, which is similar to the well-known algorithm of Wilson and Devinney (Wilson & Devinney 1971; Wilson 1979) widely used in CBS studies. Our code is described in detail in Antokhina (1988, 1996) and Antokhina et al. (2000). Here we describe its main features only. The computer code allows one to calculate light and radial velocity curves simultaneously, either for a circular or an eccentric orbit. Axial rotation of the components may be non-synchronized with the orbital revolution. Tidal and rotational distortion of the components, eclipses and possible spots on the surface of the components are taken into account. The intensity of the radiation coming from an elementary area of the stellar surface and its angular dependence are determined by the temperature of the star, gravitational darkening, limb darkening, and heating by radiation from the companion. The degree of filling the inner critical Roche lobe by a component is parametrizied by the so called Roche lobe filling factor μ, If a component completely fills its critical Roche lobe, $\mu = 1$. If the component underfills the critical Roche lobe, $\mu < 1$.

Based on the available information on the system, we set some input parameters of the model. As stated above, from the available spectral data, the estimated spectral type of
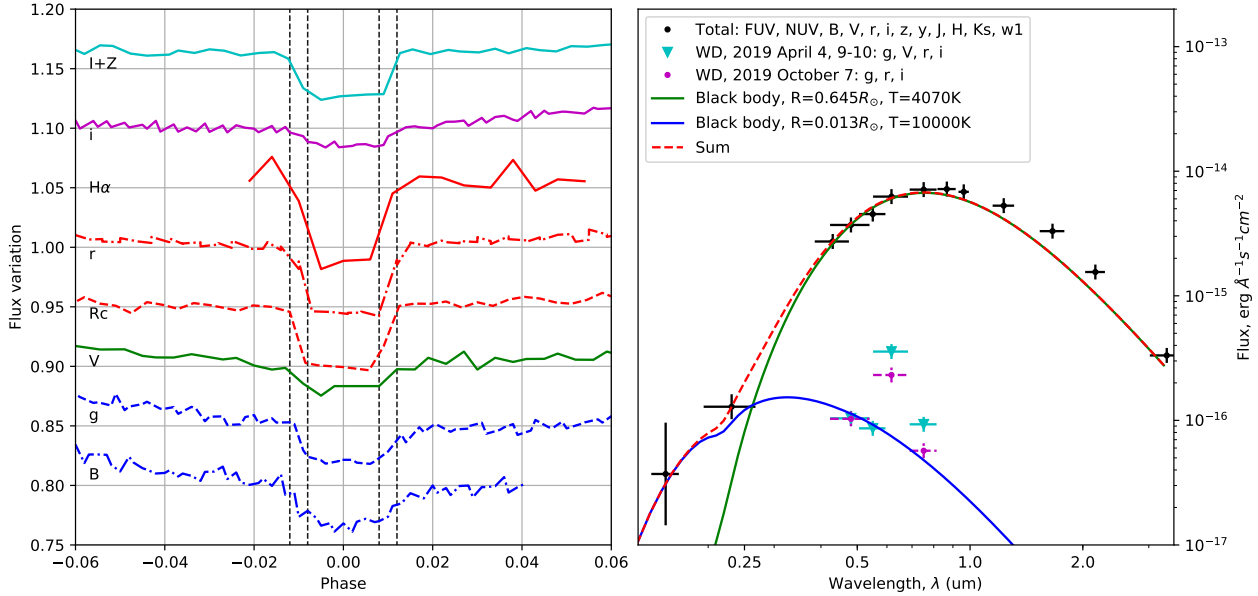
Figure 4. The WD eclipse in various bands shown on the left panel. From TRAPPIST-North: I+Z on 2018 December 5; Hα on 2018 December 12; R_C on 2018 December 10. From SAI MSU 2.5-m telescope: B on 2018 November 30. From Kourovka 1.2-m telescope: V on 2019 April 4; *SDSS g, r, i* on 2019 April 9 and 10. The ingress and egress of the eclipse is ~100s long, full duration of the eclipse is ~600s. The *GALEX* FUV and NUV, APASS B and V, PS2 *g, r, i, z* and *y*, 2MASS J, K and Ks, *WISE* w1 spectral points are shown on the right panel. Also shown are the fluxes of the eclipsed body, calculated from the depth of the eclipse for two observation sets in April and October 2019. The green and blue curves are black body models for the WD and MS components at 200 pc and $A_V = 0.31$.

the MS star is K7V. Its temperature is $T_2 \approx 4070$ K (Fig.4). The average mass of K7V stars is $M_2 \approx 0.64\,M_\odot$ (Boyajian et al. 2012). The semi-amplitude of the MS star radial velocity curve from our spectral data is $K_2 = 178\,\mathrm{km\,s^{-1}}$, which results in the mass function $f_2(m) = 0.174\,M_\odot$. Our preliminary modelling has shown that the orbital inclination angle is $i \approx 73°$. Thus, by using the third Keplerian law and the above value of the mass function, one can estimate the WD mass as $M_1 \approx 0.723\,M_\odot$ and the mass ratio as $q = M_2/M_1 \approx 0.885$. In further analysis, q was set at this value. We also used the fixed values of the gravitational darkening coefficients $\beta_1 = 0.25$ (von Zeipel 1924) and $\beta_2 = 0.08$ (Lucy 1967) as well as the albedos $A_1 = 1$ and $A_2 = 0.5$ (Ruciński 1969).

The synthetic light curves were computed in g, V, r, and i bands and fitted to the observed data. The limb darkening of the K star was accounted for by non-linear laws: the logarithmic law for g, V bands and the "square root" law for r, and i bands (van Hamme 1993). The limb darkening law and its coefficients of the WD were taken from Gianninas et al. (2013). The orbit was considered to be circular and the components rotation - synchronous with the orbital one. The orbital phases of the observed light curves were computed with our photometric ephemeris HJD = 2458762.2285 + 0.297549 days. At the orbital phase 0.0 the secondary component K7V is in front of the primary component (WD).

The variable parameters of the model are: the orbital inclination i, the Roche lobe filling factors μ_1, μ_2 and the temperature of the primary component T_1. To fit the asym-

metry of the light curve we had to add one or two spots on the K star surface with the longitude, latitude, angular radius and temperature factor as their parameters. The temperature factor is the ratio of the spot temperature to the temperature of the underlying unspotted surface (for more details of spot modelling see Wilson et al. 2017). As a rule, when fitting spot models, a fixed temperature factor is used (Wilson et al. 2017; Latković et al. 2019). Similarly to these papers, we fixed the temperature factor at 0.85 and 0.9. The difference between the spot and stellar surface temperatures is then ∼ 600 K and ∼ 400 K respectively, which corresponds to the data from Berdyugina (2005) for K stars. The well-known Simplex algorithm (Nelder & Mead 1965; Kallrath & Linnell 1987) was used when fitting the model light curve to the data. The results of the fitting are shown in Tables 4, 5 and Figs. 5 and 6. The uncertainties provided in Tables 4 and 5 are $1 - \sigma$ intervals where the true parameter values are expected to be.

In the models in g, V, i bands two model parameters are reliably defined: the orbital inclination $i \approx 73°.1$ and the K star Roche lobe filling factor $\mu_2 \approx 0.86$ (Table 4). Thus, the K star shape is tidally deformed, but the star does not fill its critical Roche lobe. This means that at the current evolutionary stage mass transfer from the K star to the WD through the inner Lagrangian point is possibly absent.

Due to the asymmetry of the light curves (Fig. 5) varying between the photometric bands the modelling was rather complicated. Note that in the g, r and i bands observations were obtained during the same night, while the data in the V band was obtained a few days earlier. Adding one spot

Table 4. Photometric solutions.

Parameter	g	V	r^a	i	Parameter status
Mass ratio $q = M_2/M_1$	0.885	0.885	0.885	0.885	adopted
Inclination i (°)	73.10 ± 0.20	73.15 ± 0.20	73.10	73.00 ± 0.20	adjusted
Roche lobe filling factor μ_1	0.017 ± 0.002	0.016 ± 0.002	0.017	0.018 ± 0.002	adjusted
Roche lobe filling factor μ_2	0.860 ± 0.010	0.865 ± 0.011	0.860	0.862 ± 0.010	adjusted
Surface potential Ω_1	161	171	161	153	computed
Surface potential Ω_2	3.991	3.973	3.991	3.984	computed
Temperature of primary T_1 (K)	8600 ± 1000	8800 ± 1000	22 000 ± 1300	14 000 ± 1000	adjusted
Temperature of secondary T_2 (K)	4070	4070	4070	4070	adopted
$L_1/(L_1 + L_2)^b$	0.029	0.016	0.056	0.012	computed
$L_2/(L_1 + L_2)^b$	0.971	0.984	0.944	0.988	computed
Spot 1 longitude (°)	164 ± 5	171 ± 6	164	192 ± 7	adjusted
Spot 1 latitude (°)	39 ± 2	35 ± 2	39	39 ± 2	adjusted
Spot 1 radius (°)	24 ± 1	29 ± 1	24	27 ± 1	adjusted
Spot 1 temp. factor	0.90	0.90	0.90	0.85	adopted
Spot 2 longitude (°)	–	60 ± 6	–	–	adjusted
Spot 2 latitude (°)	–	38 ± 5	–	–	adjusted
Spot 2 radius (°)	–	13 ± 1	–	–	adjusted
Spot 2 temp. factor	–	0.90	–	–	adopted
Relative radii (r/a)					
r_1	0.0062 ± 0.0014	0.0059 ± 0.0014	0.0062	0.0066 ± 0.0015	
$r_2(volume - averaged)$	0.3088 ± 0.0040	0.3108 ± 0.0040	0.3088	0.3095 ± 0.0040	
$r_2(pole)$	0.2975 ± 0.0057	0.3352 ± 0.0058	0.2975	0.2982 ± 0.0056	
$r_2(point)$	0.3323 ± 0.0039	0.3084 ± 0.0039	0.3323	0.3334 ± 0.0037	
$r_2(side)$	0.3064 ± 0.0034	0.2993 ± 0.0035	0.3064	0.3072 ± 0.0033	
$r_2(back)$	0.3209 ± 0.0047	0.3233 ± 0.0047	0.3209	0.3218 ± 0.0045	

^{a} Geometric parameters are fixed to those for the g band, T_1 was adjusted to fit the total eclipse.

^{b} L_1, L_2 - relative luminosities of the components

Table 5. Absolute parameters

Parameter	Value
M_1 (M$_\odot$)	0.723
M_2 (M$_\odot$)	0.640 (fixed)
a (R$_\odot$)	2.082
R_1 (R$_\odot$)	0.013 ± 0.003
R_2 (R$_\odot$)	0.645 ± 0.012
T_1 (K)	8700 ± 1100
T_2 (K)	4070 (fixed)
L_1^{bol} (L$_\odot$)	$(8.7 ± 0.2) \times 10^{-4}$
L_2^{bol} (L$_\odot$)	0.103 ± 0.003
$log(g)_1$	8.07 ± 0.21
$log(g)_2$	4.66 ± 0.02

was sufficient to fit the light curve in the g band. To fit the V curve, we had to add a small second spot on the surface of the K star. Note that **g, V** model light curves are still not in perfect agreement with the observed one with either one or two spots. The small remaining differences are possibly related to the complex spot activity of the red dwarf (for an example, see Parsons et al. 2016). We did not try to further improve the fit as it would require many more free parameters and make their values rather ambiguous. Also, the spot activity is variable over large time scale (see below). The main objective of our work was to estimate the main orbital and component parameters. Due to a unique combination of the ellipsoidal and eclipsing variability, the

geometric parameters and the WD temperature can be indeed found with high accuracy, as even a slight change in these parameters leads to strong discrepancies between the model and the observed light curves.

The r light curve is significantly different from all the others, the main differences are that the maximum at the phase ~ 0.25 is higher than the one at the phase ~ 0.75, and the eclipse is significantly deeper than that in the other bands. The out-of eclipse light curve cannot be fitted by a combination of spots on the surface of the K star, as it is highly unlikely that such spots would only demonstrate themselves in the r band alone. Moreover, no spots can explain the deep eclipse in this band. It is likely that the unusual shape of the r light curve is related to the properties of the WD. We discuss these matters below in Section 4. Thus, when computing the r model light curve, we fixed geometric parameters to those found in the g band and fitted T_1 only.

In the i band, the solution is similar to the g band, although small systematic differences between the model and the data are present in the phase interval 0.05-0.45. Adding a second spot does not improve the fit. Also, the eclipse depth is larger than it should be according to T_1 found in the bands g and V. We conclude that the differences in the i band compared to g and V are probably of the same nature as in the r band, although of smaller magnitude.

Overall, based on our modelling one can conclude that out of eclipse variability of the system is mainly determined by tidal deformation of the K star and by the presence of a low temperature spot(s) on its back half (the back half of
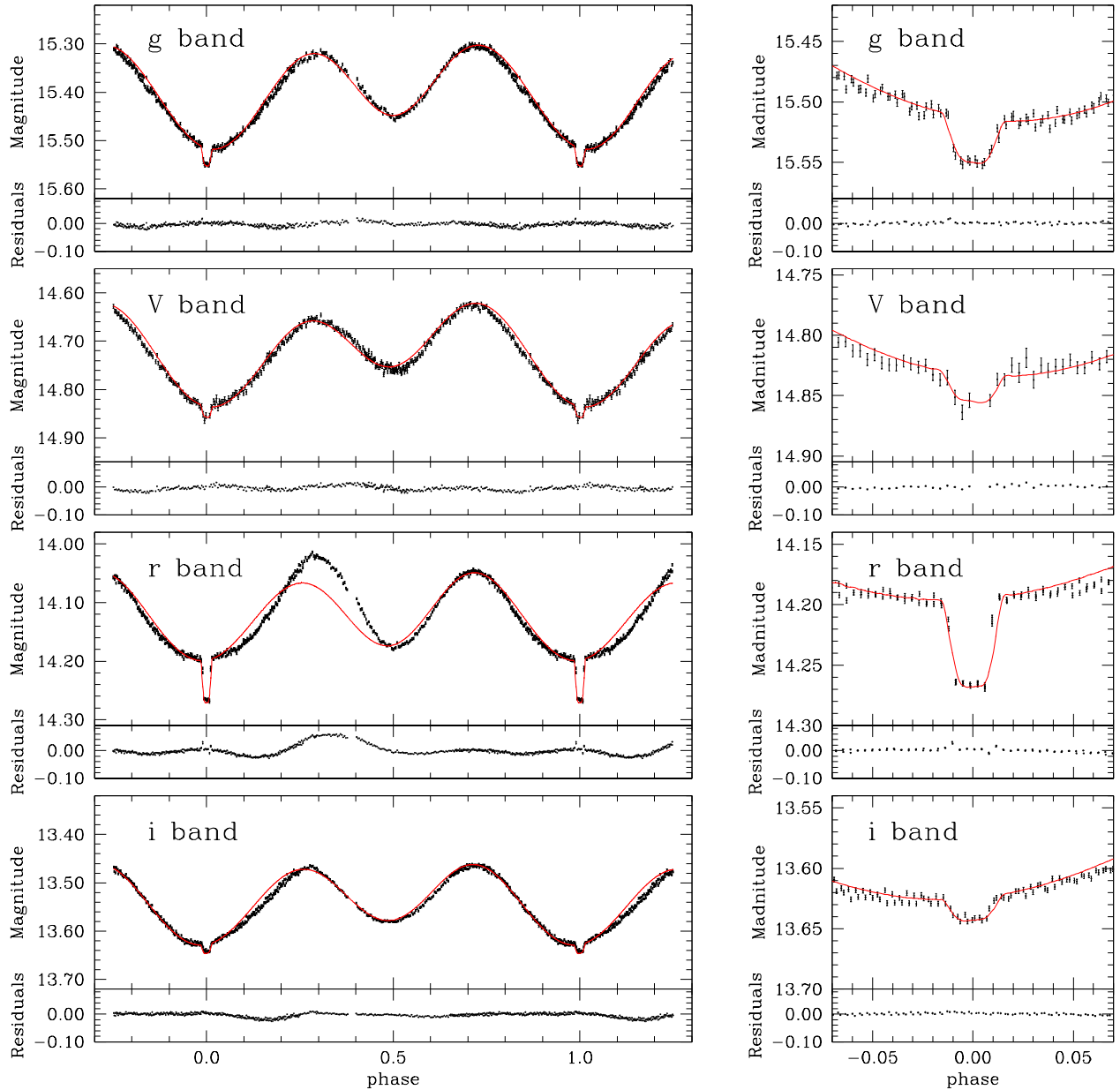
Figure 5. The light curves in the four analysed bands are shown in the left panel. The eclipse part of the light curves are in the right panel. The photometric parameters of the model solution are presented in Tables 4, 5. The observed light curve in the r band has abnormal shape. The model light curve in this band is computed with geometric parameters set to those found in the g band. T_1 was obtained by fitting the depth of the total eclipse. For details, see the text.

the star is opposite to the Lagrangian point L_1 and is visible to the observer in the orbital phase interval (approximately $0.75 - 0.40$, see Fig. 6). The reflection effect at the surface of the K star is minor, as the WD temperature is limited by $T_1 \leq 10\,000$ K (from our solution in the g, V bands as well as from *GALEX* FUV data).

The narrow total eclipse of the WD allowed us to estimate its temperature. However, as said above, it was impossible to successfully fit the eclipse in all four bands with the

same temperature. In the g and V bands the best fit is obtained with the WD temperature $T_1 = 8700 \pm 1100$ K (Fig. 5, right panel). However, in the red bands the WD temperature must be increased. While in the i band the increase is moderate ($T_1 \sim 14\,000$ K), in the r band it is much larger ($T_1 \sim 22\,000$ K). Such high values of temperature (especially $T_1 \sim 22\,000$ K in the r band) contradict the UV data which suggest that the WD temperature should be smaller than $10\,000$ K.
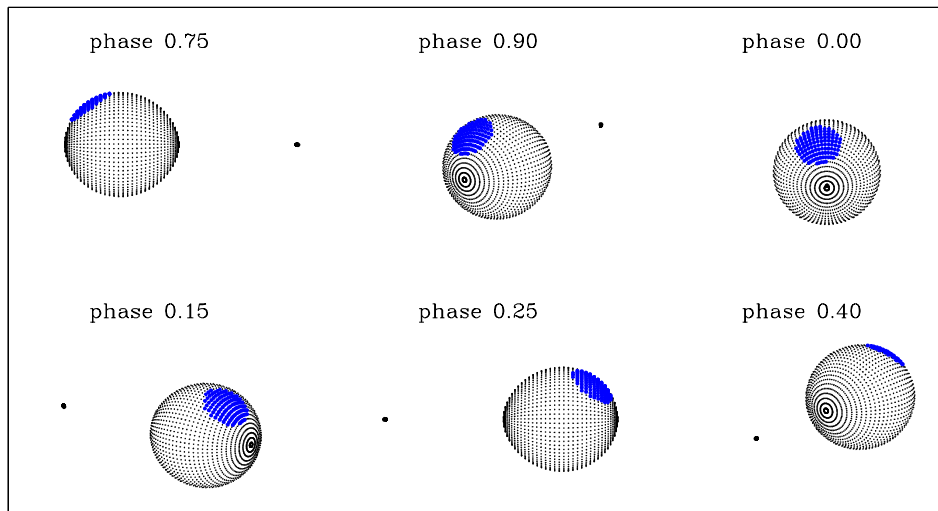
Figure 6. Model view of the binary system at the different orbital phases showing the visibility of the spot on the surface of the K star.

3.2 Light curves slow variability

We also detected slow out-of-eclipse variability of the light curve in the data gathered by the MASTER telescope simultaneously in V and R bands from January 2019 to April 2019 during 160 periods of GPX-TF16E-48. Observed variations in V and R were correlated in time. Recent additional observations in *SDSS g*, *r* and *i* filters on 2019 October 7 confirmed the variability of the light curve of the object. The changes in the elliptical variability of GPX-TF16E-48 can be explained by variations of the spot covering fractions and/or temperatures of spots on the surface of the MS companion. However, notable decrease of the depth of the eclipse in *SDSS r* and *i* filters can be related only to the properties of the eclipsed body (right panel of Fig. 4).

4 DISCUSSION

Independently of the complexities described in the previous section, the orbital inclination i and Roche lobe filling factors μ_1, μ_2 were defined with high accuracy. The ellipsoidal variability is mainly determined by a combination of i and μ_2. At the same time, the narrow total eclipse of the WD depends on i, μ_1, μ_2, T_1.

The abnormal shape of the r (and to a smaller degree, i) bands requires special discussion. As stated above, the differences in the out of eclipse light curve shape in r and other bands cannot be explained by any spots on the surface of the K star. Such spots would demonstrate themselves in all bands. Moreover, any such spots cannot explain the increased depth of the eclipse. Note that in the i band, the eclipse is also deeper than it should be at the WD temperature found from the g and V data, and the out of eclipse light curve is also deviating from the model. It seems likely that these features are related to the properties of the WD. In our model the WD temperature T_1 is just a measure of the WD luminosity (at a given WD radius). One could sug-

gest that the actual temperature is that found from g and V data, and that some additional emission of the WD is present, with the majority of the corresponding flux occurring in the r band but also demonstrating itself in the i band. It can be assumed that the excess in r is caused by Hα emission, but we did not detect strong enough lines in the spectra. Moreover, the depth of the eclipse in the Hα filter does not exceed the depth in R and *SDSS r* (left panel of Fig. 4). These facts suggest that the source of excess should have rather wide spectral features. One possible explanation could be that the WD has a strong magnetic field coupled with very low-accretion rate of stellar wind from the secondary star (the so called LARP object). These could result in cyclotron emission centered around the r band and having rather wide spectral distribution (Schwarz et al. 2001, Schwope et al. 2002, Schmidt et al. 2005, Webbink & Wickramasinghe 2005). Such a mechanism would allow us to explain the unusual spectral energy distribution of the WD (right panel of Fig. 4) (following from the depths of the eclipses in various bands) and the out of eclipse variations in the *SDSS i* and r bands. This hypothesis has an additional circumstantial evidence: significant variations of brightness of the WD on a short timescale and clear signs of strong chromospheric activity of the K star. To check this hypothesis, high S/N spectra with good time resolution and polarimetric observations are necessary. Until then, trying to fit the observed light curves in the r and i bands would be too speculative.

Obtained system parameters allowed us to make some assumptions about the past and future of the GPX-TF16E-48. Based on the current mass of the WD and the semi-empirical MIST model of initial-final mass relation of WDs from Cummings et al. 2018, the progenitor mass was close to $2.9\,M_\odot$. After the main sequence stage, the primary evolved into a red giant forming a common envelope and then into a cooling white dwarf. Using WD cooling tracks for different masses from Salaris et al. 1997 and Wood 1995 (shown in Fig. 7 of Schreiber & Gänsicke 2003), we estimated an

age of the WD as 1 Gyr. According to Verbunt & Zwaan 1981, Rappaport et al. 1983 and Schreiber & Gänsicke 2003, for the system with $M_2 > 0.3\,\mathrm{M_\odot}$ a dominant mechanism of orbital angular moment loss is a magnetic breaking. With this assumption, we can assess the orbital period at the end of the common envelope phase using Eq. (9) from Schreiber & Gänsicke 2003 as $P_{ce} \approx 1.05\,\mathrm{d}$. Due to further loss of orbital angular momentum of the system, the separation between the components will decrease and Roche lobe of secondary MS star will shrink. When the effective radius of Roche lobe reaches the radius of secondary, the system will become semi-detached, and stable mass transfer from the MS to the WD will begin. According to Eggleton 1983, and for the obtained system parameters, we derive an orbital separation and period at the beginning of semi-detached phase as $a_{sd} \approx 1.75\,\mathrm{R_\odot}$ and of $P_{sd} \approx 5.5\,\mathrm{hours}$ respectively. The time before the onset of the semi-detached phase calculated by Eq. (9) from Schreiber & Gänsicke 2003 is $t_{sd} \approx 8.9 \times 10^6$ years.

5   CONCLUSIONS

The discovery and the results of the follow-up observations and preliminary light curve modelling of the bright eclipsing post-common envelope binary GPX-TF16E-48 are presented. It is shown that the system consists of a cool white dwarf (WD) and a K7V star.

Based on our analysis of the spectral and photometric data, we estimated the parameters of the system. The K7V star is tidally deformed but does not fill its Roche lobe ($\mu_2 \approx 0.86$). The orbital inclination $i = 73°.1 \pm 0°.2$ and the mass ratio $q = M_2/M_1 \approx 0.88$. The parameters of the K7V star are $M_2 \approx 0.64\,\mathrm{M_\odot}$ (adopted from the average mass of K7V stars, Boyajian et al. 2012), $R_2 = 0.645 \pm 0.012\,\mathrm{R_\odot}$, and $T_2 \approx 4070\,\mathrm{K}$. Note that the obtained radius of the K7V star is close to the typical radius ($0.65\,\mathrm{R_\odot}$) from Boyajian et al. (2012). The parameters of the white dwarf are $M_1 \approx 0.72\,\mathrm{M_\odot}$, $R_1 = 0.013 \pm 0.003\,\mathrm{R_\odot}$, $T_1 = 8700 \pm 1100\,\mathrm{K}$.

The depth of eclipse in various bands revealed unusual spectral energy distribution of the eclipsed body. In the case of an eclipsing WDMS system, the depths of the eclipse observed in different bands vary and they are determined by the ratio of temperatures of the components. For a typical system, which consists of a late red dwarf and a WD, observed eclipse depths increase from IR to UV (Maxted et al. 2004; Law et al. 2012; Parsons et al. 2013b; Latković et al. 2019). However, in the case of GPX-TF16E-48, multi-colour photometric follow-up observations revealed that depths of eclipses show an unusual colour dependence with an excess in red filters (see Fig. 2 and Fig. 4). Also, a change of the depth of total eclipse was detected, which occur in a monthly timescale.

We suspect that the primary (WD) companion of GPX-TF16E-48 has a strong magnetic field and accrete stellar wind from the secondary companion at a low rate. These could result in cyclotron emission, which dominates in the observed range of the WD spectrum. Additional photometric, spectroscopic and polarimetric observations with high time resolution are necessary to determine the real nature of the GPX-TF16E-48. The object will be observed by TESS (Ricker et al. 2014) in Sector 18 from 2019 November 02

to 2019 November 27 (TIC 353075202, TESS mag $= 13.15$). Though TESS data is gathered in just one filter, it will be useful to look for possible eclipse timing and shape variations, the spot and chromospherical activity of the K7V companion.

REFERENCES

Antokhina E. A., 1988, Soviet Ast., 32, 608
Antokhina E. A., 1996, Astronomy Reports, 40, 483
Antokhina E. A., Moffat A. F. J., Antokhin I. I., Bertrand J.-F., Lamontagne R., 2000, ApJ, 529, 463
Barkaoui K., Gillon M., Benkhaldoun Z., Emmanuel J., Elhalkouj T., Daassou A., Burdanov A., Delrez L., 2017, in Journal of Physics Conference Series. p. 012073, doi:10.1088/1742-6596/869/1/012073
Benni P., 2017, Journal of the American Association of Variable Star Observers (JAAVSO), 45, 127
Berdyugina S. V., 2005, Living Reviews in Solar Physics, 2, 8
Borucki W. J., et al., 2010, Science, 327, 977
Boyajian T. S., et al., 2012, ApJ, 757, 112
Bruch A., Diaz M. P., 1998, AJ, 116, 908
Burdanov A. Y., Krushinsky V. V., Popov A. A., 2014, Astrophysical Bulletin, 69, 368
Burdanov A. Y., et al., 2016, MNRAS, 461, 3854
Burdanov A., et al., 2018, PASP, 130, 074401

Chambers K. C., et al., 2016, arXiv e-prints,

Cummings J. D., Kalirai J. S., Tremblay P. E., Ramirez-Ruiz E., Choi J., 2018, ApJ, 866, 21

Drake A. J., et al., 2009, ApJ, 696, 870

Eggleton P. P., 1983, ApJ, 268, 368

Faigler S., Kull I., Mazeh T., Kiefer F., Latham D. W., Bloemen S., 2015, ApJ, 815, 26

Gaia Collaboration et al., 2018, A&A, 616, A1

Gianninas A., Strickland B. D., Kilic M., Bergeron P., 2013, ApJ, 766, 3

Gillon M., Jehin E., Magain P., Chantry V., Hutsemékers D., Manfroid J., Queloz D., Udry S., 2011, in European Physical Journal Web of Conferences. p. 06002 (arXiv:1101.5807), doi:10.1051/epjconf/20101106002

Henden A. A., Levine S., Terrell D., Welch D. L., 2015, in American Astronomical Society Meeting Abstracts #225. p. 336.16

Jehin E., et al., 2011, The Messenger, 145, 2

Kallrath J., Linnell A. P., 1987, ApJ, 313, 346

Knigge C., Baraffe I., Patterson J., 2011, ApJS, 194, 28

Lafler J., Kinman T. D., 1965, ApJS, 11, 216

Lang D., Hogg D. W., Mierle K., Blanton M., Roweis S., 2010, The Astronomical Journal, 139, 1782âĂŞ1800

Latković O., Cséki A., Djurašević G., Essam A., Hamed A. S., Youssef S. M., 2019, AJ, 157, 3

Law N. M., et al., 2012, ApJ, 757, 133

Lipunov V., et al., 2010, Advances in Astronomy, 2010, 349171

Lucy L. B., 1967, Z. Astrophys., 65, 89

Maxted P. F. L., Marsh T. R., Morales-Rueda L., Barstow M. A., Dobbie P. D., Schreiber M. R., Dhillon V. S., Brinkworth C. S., 2004, MNRAS, 355, 1143

Maxted P. F. L., et al., 2014, MNRAS, 437, 1681

Nelder J. A., Mead R., 1965, The Computer Journal, 7, 308

Paczynski B., 1976, in Eggleton P., Mitton S., Whelan J., eds, IAU Symposium Vol. 73, Structure and Evolution of Close Binary Systems. p. 75

Parsons S. G., et al., 2013a, MNRAS, 429, 256

Parsons S. G., Marsh T. R., Gänsicke B. T., Schreiber M. R., Bours M. C. P., Dhillon V. S., Littlefair S. P., 2013b, MNRAS, 436, 241

Parsons S. G., et al., 2015, MNRAS, 449, 2194

Parsons S. G., et al., 2016, MNRAS, 458, 2793

Parsons S. G., et al., 2017, MNRAS, 470, 4473

Pollacco D. L., et al., 2006, PASP, 118, 1407

Potanin S. A., Gorbunov I. A., Dodin A. V., Savvin A. D., Safonov B. S., Shatsky N. I., 2017, Astronomy Reports, 61, 715

Pyrzas S., et al., 2009, MNRAS, 394, 978

Rappaport S., Verbunt F., Joss P. C., 1983, ApJ, 275, 713

Ren J. J., Rebassa-Mansergas A., Parsons S. G., Liu X. W., Luo A. L., Kong X., Zhang H. T., 2018, MNRAS, 477, 4641

Ricker G. R., et al., 2014, in Space Telescopes and Instrumentation 2014: Optical, Infrared, and Millimeter Wave. p. 914320 (arXiv:1406.0151), doi:10.1117/12.2063489

Rose M. B., Hintz E. G., 2007, The Astronomical Journal, 134, 2067

Ruciński S. M., 1969, Acta Astron., 19, 245

Salaris M., Domínguez I., García-Berro E., Hernanz M., Isern J., Mochkovitch R., 1997, ApJ, 486, 413

Schmidt G. D., et al., 2005, ApJ, 630, 1037

Schreiber M. R., Gänsicke B. T., 2003, A&A, 406, 305

Schwarz R., Schwope A. D., Staude A., 2001, A&A, 374, 189

Schwope A. D., Brunner H., Hambaryan V., Schwarz R., 2002, in Gänsicke B. T., Beuermann K., Reinsch K., eds, Astronomical Society of the Pacific Conference Series Vol. 261, The Physics of Cataclysmic Variables and Related Objects. p. 102

Skrutskie M. F., et al., 2006, AJ, 131, 1163

Tappert C., Gänsicke B. T., Schmidtobreick L., Aungwerojwit A., Mennickent R. E., Koester D., 2007, A&A, 474, 205

Tody D., 1993, IRAF in the Nineties. p. 173

Valdes F., Gupta R., Rose J. A., Singh H. P., Bell D. J., 2004, ApJS, 152, 251

Verbunt F., Zwaan C., 1981, A&A, 100, L7

Webbink R. F., Wickramasinghe D. T., 2005, in Hameury J. M., Lasota J. P., eds, Astronomical Society of the Pacific Conference Series Vol. 330, The Astrophysics of Cataclysmic Variables and Related Objects. p. 137

Willems B., Kolb U., 2004, A&A, 419, 1057

Wilson O. C., 1968, ApJ, 153, 221

Wilson R. E., 1979, ApJ, 234, 1054

Wilson R. E., Devinney E. J., 1971, ApJ, 166, 605

Wilson R. E., Pilachowski C. A., Terrell D., 2017, ApJ, 835, 251

Wood M. A., 1995, Theoretical White Dwarf Luminosity Functions: DA Models. p. 41, doi:10.1007/3-540-59157-5_171

York D. G., et al., 2000, AJ, 120, 1579

van Hamme W., 1993, AJ, 106, 2096

von Zeipel H., 1924, MNRAS, 84, 702

This paper has been typeset from a TEX/LATEX file prepared by the author.